ROYAL SOCIETY OF CHEMISTRY

PAPER

Check for updates

Temperature dependent Raman study of antiferromagnetic CrPS₄†

Manh Hong Nguyen,[a] Suhan Son,[b] Giung Park,[b] Woongki Na,[a] Je-Geun Park [ID] *[b] and Hyeonsik Cheong [ID] *[a]

The temperature dependence of the Raman spectrum of exfoliated CrPS₄ samples was investigated by polarized Raman spectroscopy with three excitation sources between 4 K and room temperature (293 K). The peak positions and the polarization dependences of the 14 observed Raman modes are consistent with the previous report at room temperature. However, there are some critical changes in the Raman spectrum at low temperatures. For the bulk sample, the mode at ∼306 cm⁻¹ is polarized along the b-axis of the crystal at room temperature but is slightly polarized along the a-axis at low temperatures. In addition, a mode at ∼188 cm⁻¹ emerges, and its intensity increases dramatically below the Néel temperature. Both of these changes were most prominent with a 2.41 eV excitation source. Similar changes were observed in few-layer samples down to 2-layers.

1. Introduction

Magnetic van der Waals (vdW) materials have been intensively studied because they have diverse and controllable properties that offer them a lot of potential for electronic and spintronic applications.[1–3] For example, the magnetoresistance of ferromagnetic Fe₃GeTe₂ depends on the thickness,[4] and the magnetic properties of CrI₃ few-layer samples show either ferromagnetic or antiferromagnetic ordering when the sample has odd or even layers, respectively.[5] The transition metal phosphorus sulfide (MPS₃, M = Fe, Mn, and Ni) family exhibits antiferromagnetic ordering. However, their magnetic structure depends on the transition metal element: FePS₃ is an Ising-zigzag type, MnPS₃ is a Heisenberg type, and NiPS₃ is an XXZ type.[6–9] Raman spectroscopy has been proven a powerful tool for studying various properties of van der Waals materials, such as thickness, interlayer interactions, or the effect of twist angles.[10] In particular, Raman spectroscopy has been very useful in studying the magnetic properties of van der Waals magnetic materials.[11–15]

Recently, semiconducting CrPS₄ with an optical bandgap of 1.4 eV has attracted much interest because it can be exfoliated down to a monolayer, and the material is air-stable.[16–22] It is an A-type antiferromagnet with the spins in one layer showing out-of-plane

Ising-type ferromagnetic ordering with the antiferromagnetic ordering of the spins in alternating layers. The Néel temperature (T_N) is at about 38 K in the bulk and 23 K in few-layer flakes.[16,18,21] In temperature-dependent photoluminescence (PL) studies on bulk samples, Fano resonances that correlate with the magnetic phase transition have been observed.[22–24] In magneto-optic Kerr effect (MOKE) measurements, the magnetic transition of ferromagnetic odd-layer samples was measured, and the critical temperature was not sensitively dependent on the number of layers for 1, 3, and 5-layer samples.[16] The Raman and infrared measurements of the phonon modes in CrPS₄ have been studied at room temperature: Kim *et al.* performed polarized Raman spectroscopy and calculated the Raman tensor of bulk CrPS4;[25] Lee *et al.* recorded the Raman spectrum of few-layer CrPS₄ down to the monolayer,[19] and Neal *et al.* used the first-principles density functional theory calculations to figure out the vibrational modes.[26] The temperature dependence of bulk CrPS₄ has also been studied by Gu *et al.*, but they did not find any correlation between the Raman spectrum and the magnetic phase transition.[22] So far, studies on the temperature dependence and the polarization behaviors of the phonon modes and the correlation with the magnetic transition have been lacking.

In this work, we report the temperature dependence of the Raman spectrum of few-layer and bulk CrPS₄ with 3 excitation energies. The polarization dependences are also compared as a function of temperature. The appearance of a mode at ∼188 cm⁻¹ correlates with the magnetic ordering below the Néel temperature. The polarization behavior of the Raman mode at ∼306 cm⁻¹ changes dramatically as the

[a] Department of Physics, Sogang University, Seoul 04107, Korea.
  E-mail: hcheong@sogang.ac.kr
[b] Department of Physics and Astronomy, Seoul National University, Seoul 08826, Korea. E-mail: jgpark10@snu.ac.kr

sample is cooled below the Néel temperature when the 2.41 eV excitation is used.

2. Experimental

Sample fabrication

Bulk single-crystal $CrPS_4$ was fabricated using the chemical vapor transport method.[16] Samples were mechanically exfoliated from the bulk crystal onto 280 nm SiO_2/Si substrates. The sample thickness was measured by atomic force microscopy (AFM). The thickness of one $CrPS_4$ layer is about 0.6 nm, consistent with previous publications (see Fig. S1, ESI†).[16] The as-prepared samples were stored in a vacuum chamber in order to avoid any possible degradation in air.

Raman measurements

Raman measurements were conducted with excitation energies of 1.96 eV (He–Ne laser), 2.41 eV (diode-pumped solid-state laser), and 2.71 eV (Ar-ion laser). The beam was focused onto the samples by a 40× objective lens (N.A. 0.6), and the laser power was kept below 100 µW to avoid heating damage. The scattered light was dispersed using a Jobin-Yvon Horiba iHR550 spectrometer (1200 groves per mm blazed at 630 nm for the 1.96 eV excitation and 2400 groves per mm blazed at 400 nm for the 2.41 eV and 2.71 eV excitations) and detected using a liquid-nitrogen-cooled back-illuminated charged-coupled-device (CCD). All the polarizations of the incident and scattered light were controlled by a set of two polarizers and two half-wave plates. The polarization angle (θ) was measured with respect to the a-axis of the crystal, by comparing the polarization dependence of the Raman modes in previous reports.[25,27] During the measurements, samples were kept in a closed-cycle He cryostat (Montana).

3. Results and discussion

Fig. 1(a) illustrates the crystal structure of $CrPS_4$ with the lattices constant a = 10.871 Å, b = 7.254 Å, c = 6.140 Å, and the angle between a- and c-axes β = 91.88°, which is monoclinic with the space group C_2^3 (Z = 4, four formulae per unit cell).[21,28] The P atom bonds to 4 S atoms to form a tetrahedron PS_4. The Cr atom and six adjacent S atoms form a slightly distorted octahedron of CrS_6. The CrS_6 octahedrons share their edges and form chains along the b-axis.[28] A group theoretical analysis shows that $CrPS_4$ has 36 vibrational modes, including 17 A-symmetry modes and 19 B-symmetry modes, which are Raman-active except for the three acoustic-phonon modes (1A + 2B).[19,25,26] The Raman tensors are[29]

$$R(\mathrm{A}) = \begin{pmatrix} a & 0 & d \\ 0 & b & 0 \\ d & 0 & c \end{pmatrix} \quad \text{and} \quad R(\mathrm{B}) = \begin{pmatrix} 0 & e & 0 \\ f & 0 & f \\ 0 & e & 0 \end{pmatrix}.$$

In the backscattering geometry on the ab plane, the A and B-type modes are only observed in parallel $[\bar{z}(xx)z]$, $[\bar{z}(yy)z]$ and cross $[\bar{z}(xy)z]$ polarized Raman spectra, respectively. Here, z and $\bar{z}$ refer to the propagation directions of the incident and scattered photons, and the two labels inside the parenthesis refer to the polarization directions of the incident and scattered photons, respectively. We set the $x(y)$-direction along the $a(b)$-axis of the crystal. Fig. 1(b) shows the polarized Raman spectra of a bulk $CrPS_4$ sample at low temperature (4 K) and room temperature (293 K) measured in $[\bar{z}(xx)z]$, $[\bar{z}(yy)z]$ and $[\bar{z}(xy)z]$ polarizations with the 2.41 eV excitation. At 293 K, we observed 6 A modes and 7 B modes below 360 cm^{-1}, consistent with previous publications.[19,25] On the other hand, at 4 K, another A mode (A3) at $\sim$188 cm^{-1} is resolved. At 293 K, this mode is also very weak with the 2.71 eV excitation but is visible with the
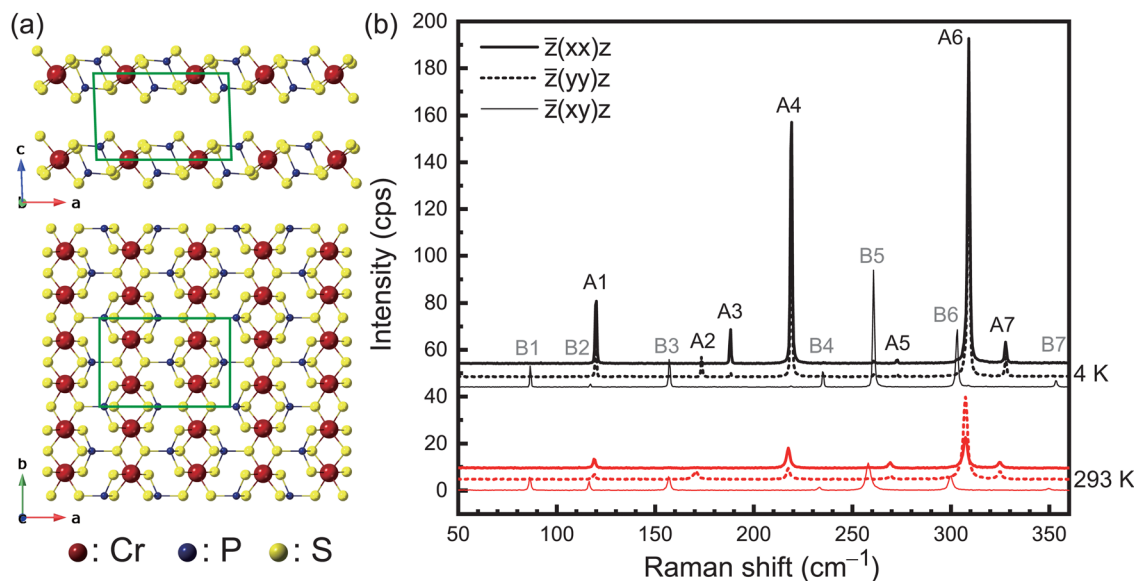

Fig. 1 (a) Crystal structure of $CrPS_4$, side view and top view. The green rectangle indicates the unit cell. (b) Raman spectra of a bulk $CrPS_4$ sample at 4 K (black) and room-temperature (red), measured with the 2.41 eV excitation source in the parallel $[\bar{z}(xx)z]$ (thick lines), $[\bar{z}(yy)z]$ (dotted lines) and cross $[\bar{z}(xy)z]$ (thin lines) polarization configurations. The labels indicate the A- and B-type Raman modes of $CrPS_4$.
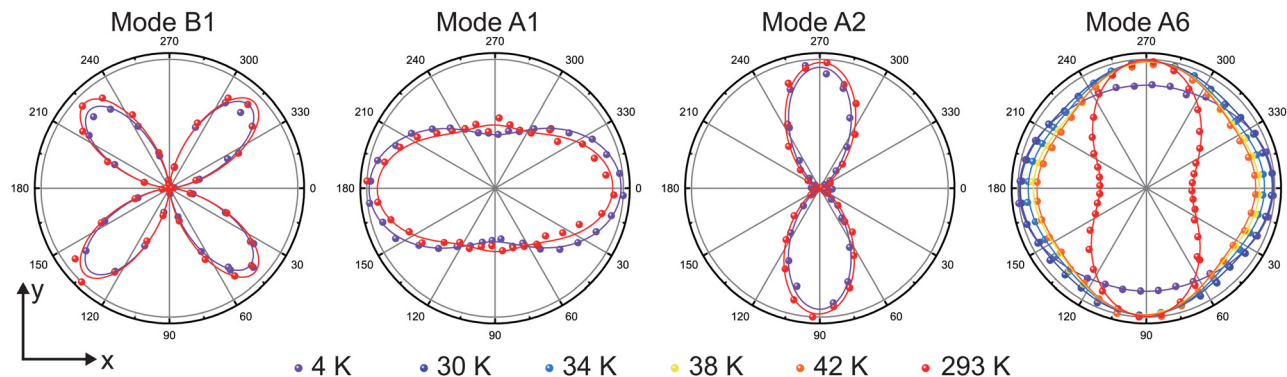
This journal is © The Royal Society of Chemistry 2024

J. Mater. Chem. C, 2024, **12**, 12468–12473 | **12469**

Fig. 2 Polarization dependence of select Raman modes in CrPS$_4$ at select temperatures. The dots and lines are experimental data and fitting, respectively. These data were collected with the 2.41 eV excitation source.

1.96 eV excitation. The observed Raman modes are compared with the calculated phonon modes in Table S1 (ESI†).[26] Its intensity also increases at 4 K with the 1.96 and 2.71 eV excitations. However, for the 1.96 eV excitation, the polarization direction is orthogonal to the 2.41 eV case (see Fig. S2, ESI†).
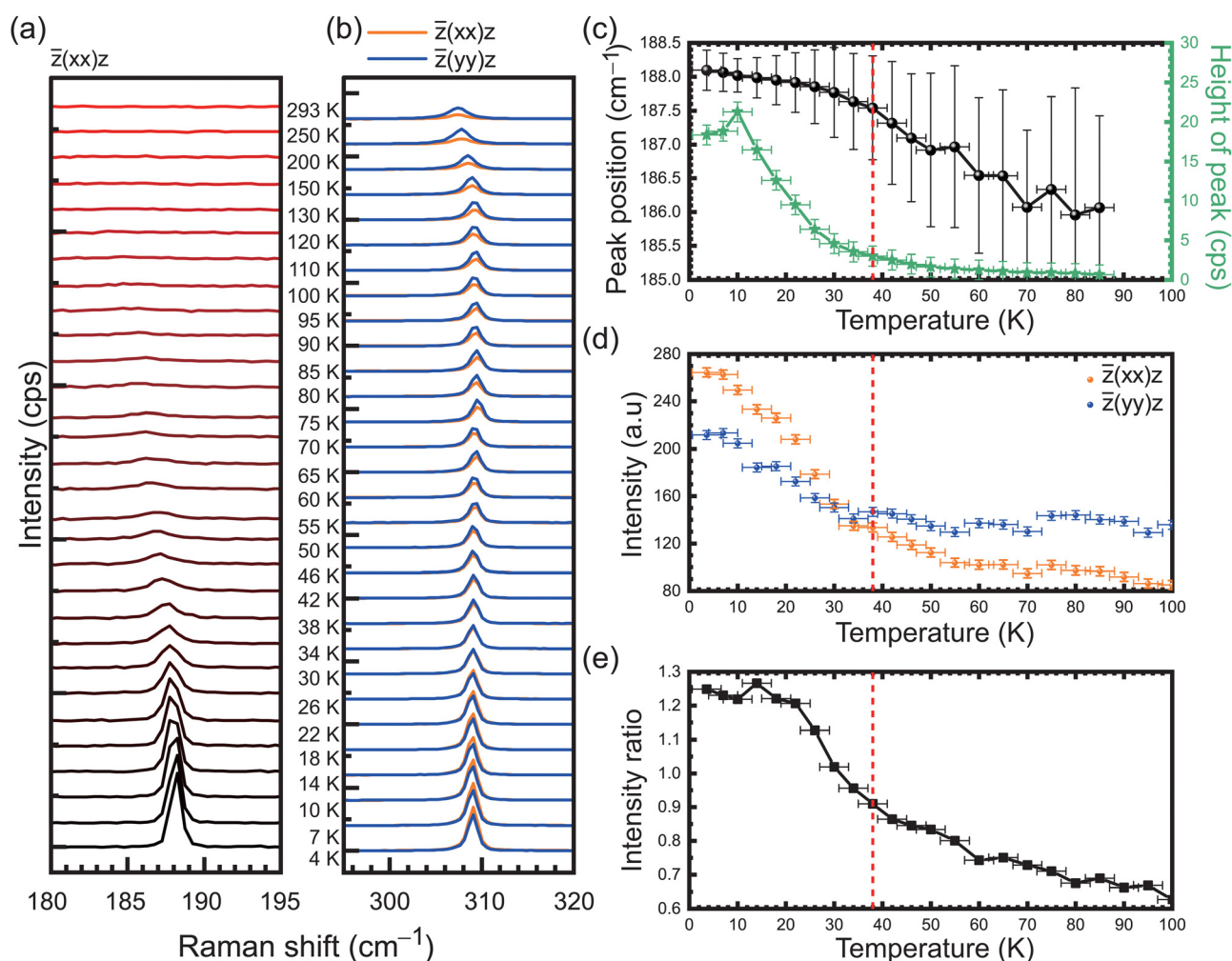

Fig. 3 (a) Temperature dependence of the A3 mode of a bulk sample. (b) Temperature dependence of the A6 mode of a bulk sample for two different polarizations. The Raman spectra were recorded with the 2.41 eV excitation. (c) Temperature dependence of the peak position (black) and the height (green) extracted from (a). (d) Temperature dependence of the intensity of A6 for two different polarizations of [$\bar{z}(xx)z$] (orange) and [$\bar{z}(yy)z$] (blue). (e) Temperature dependence of the intensity ratio of the two polarizations in (d). The vertical red dashed lines indicate the Néel temperature of 38 K. The error bars indicate the experimental uncertainties.

12470 | *J. Mater. Chem. C*, 2024, **12**, 12468–12473

This journal is © The Royal Society of Chemistry 2024

The polarization dependences of the Raman modes at room temperature and at 4 K are shown in Fig. 2, Fig. S3 and S4 (ESI†). Here, the polarizations of the incident and scattered photons are parallel and a half-wave plate is used to rotate the polarization of incident photons with respect to the crystal axes. In the polar plot, $0°$ corresponds to the *a*-axis. The B-type modes show the characteristic 4-fold polarization dependence that does not change at low temperatures. On the other hand, the A-type modes show rather complex polarization dependences that depend on the temperature and the excitation energy. Such a behavior is often observed in 2-dimensional materials with in-plane anisotropy and is consistent with the previous report on $CrPS_4$.[25,30–32] Qi *et al.* used the polarization of mode A2 to find the *b*-axis.[27] At 4 K, there are some changes in the polarization dependences of some of the A modes, whereas those of A1 and A2 do not change much (Fig. 2 and Fig. S3, ESI†). The changes are most dramatic for the A6 mode: the intensity is maximum along the *b*-axis at room temperature but is almost isotropic with the maximum along the *a*-axis at 4 K. Kim *et al.* reported that at room temperature, the A6 mode is polarized along the *a*-axis for the 1.96 eV excitation and along the *b*-axis for 2.41 and 2.71 eV excitations.[25] We observed the same excitation dependence but also discovered that the polarization direction changes between room temperature and 4 K only for the 2.41 eV (see Fig. 2 and Fig. S5, ESI†). Louisy *et al.* reported that the lowest energy optical transition due to a d–d type transition is at 1.4 eV, but the fundamental charge transfer or bandgap transition is at ~ 2.4 eV.[21] Therefore, we can infer that the observed excitation energy dependence may be explained by the resonance with the transition at ~ 2.4 eV. The temperature dependence of the A6 mode for the 2.41 eV excitation may also result from such a resonance. The bandgap energy generally changes as the temperature changes, modifying the resonance conditions. Such changes would be more dramatic if the excitation is close to the bandgap energy. If the material goes through a magnetic transition, it will also modify the band structure, resulting in further changes in the resonance conditions.

Fig. 3(a) shows the temperature dependence of the A3 mode. At room temperature, this mode is almost invisible with 2.41 eV. Its temperature dependence is summarized in Fig. 3(c). It becomes visible as the temperature is lowered toward the Néel temperature, and the intensity increases dramatically below it. Fig. 3(b) shows the temperature dependence of the A6 mode for $[\bar{z}(xx)z]$ and $[\bar{z}(yy)z]$. The peak blue shifts slightly from ~ 306 cm^{-1} at room temperature to ~ 309 cm^{-1} at 4 K. The polarization dependence of this mode changes with temperature, and Fig. 3(d) and (e) summarize the ratio between the intensities measured in two different polarizations. As the temperature is cooled below the Néel temperature, the intensities are reversed, as we have seen in Fig. 2. Recently, Qi *et al.* studied the anisotropic magnon transport in $CrPS_4$ and found that the magnon transport is stronger along the *b*-axis.[27] This suggests that the change in the polarization of the A6 mode as the material goes through magnetic ordering may be explained in terms of the phonon–magnon coupling. Further studies are needed to elucidate such coupling effects.
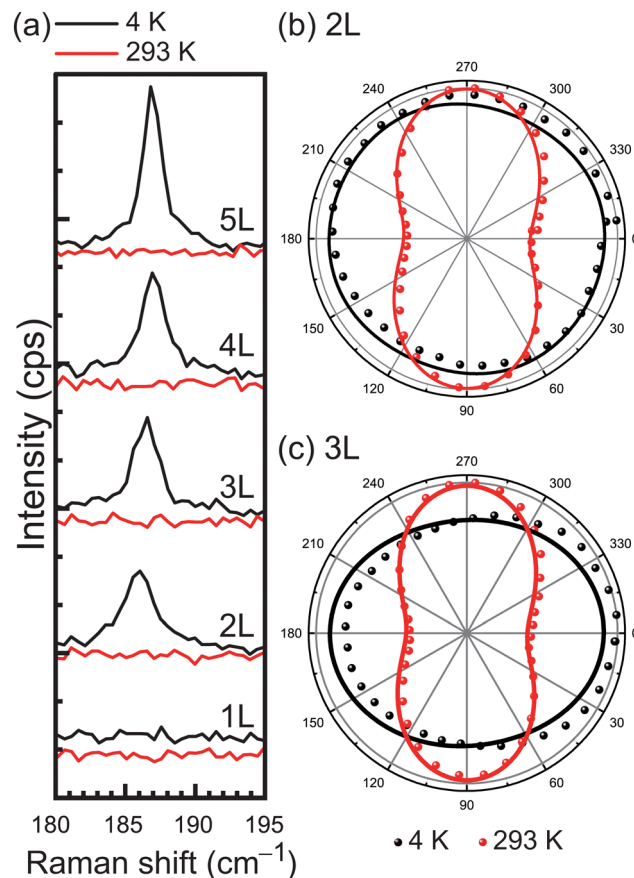

Fig. 4 (a) A3 mode of 1L, 2L, 3L, 4L and 5L $CrPS_4$ samples. (b) and (c) Polarization dependences of the A6 mode of 2L and 3L $CrPS_4$ at 4 K (black) and 293 K (red), respectively. The dots and lines are experimental data and fitting, respectively. These data were recorded with the 2.41 eV excitation.

We studied the thickness dependence of the Raman spectra of few-layer $CrPS_4$ samples using the 2.41 eV excitation, which showed the most dramatic changes in the Raman spectrum through the antiferromagnetic transition. We obtained high-resolution Raman spectra down to 2L (see Fig. S7, ESI†), and the peak positions and linewidths are consistent with previous results.[19] From the monolayer (1L) sample, we could resolve only a couple of very weak peaks, which is consistent with previous reports.[16,19,33] It has been reported that the $CrPS_4$ monolayer is prone to degradation in air, although the bulk material is known to be air-stable.[33] On the other hand, the magnetic transition could be observed in the MOKE measurements on such 1L samples.[16] Since Raman scattering is more sensitive to the imperfections in the crystal than MOKE, this may indicate that the crystallinity of the 1L sample was not good enough. In 1L $MnPS_3$, which is more sensitive to air exposure, the Raman modes were similarly very weak. In contrast, other magnetic van der Waals materials, such as $FePS_3$ and $NiPS_3$, show well-resolved Raman modes down to 1L.[11,13,15] The emergence of the A3 mode and the change in the polarization dependence of the A6 mode as the temperature is lowered through the Néel temperature are observed as in

the case of the bulk material (see Fig. S8 to S11, ESI†). Fig. 4 summarizes such results.

4. Conclusion

In summary, the polarized Raman spectrum of $CrPS_4$ measured with a 2.41 eV excitation source exhibits two major changes as the sample is cooled below the Néel temperature: the A3 mode at ~ 188 cm^{-1} is greatly enhanced, and the polarization of the A6 mode at ~ 306 cm^{-1} changes dramatically. These changes are not as pronounced with the other excitation energies (1.96 and 2.71 eV), suggesting a resonance effect. The same measurements were carried out on few-layer $CrPS_4$ samples, and similar effects were observed down to 2 layers. Our findings indicate that there is intricate correlation between the phonon modes and the magnetic ordering and provide valuable information for future work on $CrPS_4$: one should be careful in using the polarized Raman measurements to determine the crystal axes as the polarizations of some of the modes depend on the temperature as well as the excitation laser energy.

Author contributions

H. C. conceived the measurements. S. S. and G. P. prepared the single-crystal bulk sample under the guidance of J. G. P. M. H. N. prepared few-layer samples and carried out the AFM. M. H. N. and W. N. carried out the Raman measurements. M. H. N., W. N. and H. C. analyzed the data and prepared the manuscript.

Data availability

The data supporting this article have been included as part of the main article and the ESI.† The raw data may be obtained from the corresponding authors upon reasonable request.

Conflicts of interest

The authors declare no competing financial interests.

Acknowledgements

References

1 X. Jiang, Q. Liu, J. Xing, N. Liu, Y. Guo, Z. Liu and J. Zhao, *Appl. Phys. Rev.*, 2021, **8**, 031305.

2 Q. H. Wang, A. Bedoya-Pinto, M. Blei, A. H. Dismukes, A. Hamo, S. Jenkins, M. Koperski, Y. Liu, Q.-C. Sun, E. J. Telford, H. H. Kim, M. Augustin, U. Vool, J.-X. Yin, L. H. Li, A. Falin, C. R. Dean, F. Casanova, R. F. L. Evans, M. Chshiev, A. Mishchenko, C. Petrovic, R. He, L. Zhao, A. W. Tsen, B. D. Gerardot, M. Brotons-Gisbert, Z. Guguchia, X. Roy, S. Tongay, Z. Wang, M. Z. Hasan, J. Wrachtrup, A. Yacoby, A. Fert, S. Parkin, K. S. Novoselov, P. Dai, L. Balicas and E. J. G. Santos, *ACS Nano*, 2022, **16**, 6960–7079.

3 J.-G. Park, *J. Phys.: Condens. Matter*, 2016, **28**, 301001.

4 C. Tan, J. Lee, S.-G. Jung, T. Park, S. Albarakati, J. Partridge, M. R. Field, D. G. McCulloch, L. Wang and C. Lee, *Nat. Commun.*, 2018, **9**, 1554.

5 B. Huang, G. Clark, E. Navarro-Moratalla, D. R. Klein, R. Cheng, K. L. Seyler, D. Zhong, E. Schmidgall, M. A. McGuire, D. H. Cobden, W. Yao, D. Xiao, P. Jarillo-Herrero and X. Xu, *Nature*, 2017, **546**, 270–273.

6 P. A. Joy and S. Vasudevan, *Phys. Rev. B: Condens. Matter Mater. Phys.*, 1992, **46**, 5425–5433.

7 P. Jernberg, S. Bjarman and R. Wäppling, *J. Magn. Magn. Mater.*, 1984, **46**, 178–190.

8 S. Y. Kim, T. Y. Kim, L. J. Sandilands, S. Sinn, M.-C. Lee, J. Son, S. Lee, K.-Y. Choi, W. Kim, B.-G. Park, C. Jeon, H.-D. Kim, C.-H. Park, J.-G. Park, S. J. Moon and T. W. Noh, *Phys. Rev. Lett.*, 2018, **120**, 136402.

9 K. Okuda, K. Kurosawa, S. Saito, M. Honda, Z. Yu and M. Date, *J. Phys. Soc. Jpn.*, 1986, **55**, 4456–4463.

10 X. Cong, X.-L. Liu, M.-L. Lin and P.-H. Tan, *npj 2D Mater. Appl.*, 2020, **4**, 13.

11 J.-U. Lee, S. Lee, J. H. Ryoo, S. Kang, T. Y. Kim, P. Kim, C.-H. Park, J.-G. Park and H. Cheong, *Nano Lett.*, 2016, **16**, 7433–7438.

12 K. Kim, S. Y. Lim, J. Kim, J.-U. Lee, S. Lee, P. Kim, K. Park, S. Son, C.-H. Park, J.-G. Park and H. Cheong, *2D Mater.*, 2019, **6**, 041001.

13 K. Kim, S. Y. Lim, J.-U. Lee, S. Lee, T. Y. Kim, K. Park, G. S. Jeon, C.-H. Park, J.-G. Park and H. Cheong, *Nat. Commun.*, 2019, **10**, 345.

14 W. Jin, H. H. Kim, Z. Ye, S. Li, P. Rezaie, F. Diaz, S. Siddiq, E. Wauer, B. Yang, C. Li, S. Tian, K. Sun, H. Lei, A. W. Tsen, L. Zhao and R. He, *Nat. Commun.*, 2018, **9**, 5122.

15 S. Y. Lim, K. Kim, S. Lee, J.-G. Park and H. Cheong, *Curr. Appl. Phys.*, 2021, **21**, 1–5.

16 J. Son, S. Son, P. Park, M. Kim, Z. Tao, J. Oh, T. Lee, S. Lee, J. Kim, K. Zhang, K. Cho, T. Kamiyama, J. H. Lee, K. F. Mak, J. Shan, M. Kim, J.-G. Park and J. Lee, *ACS Nano*, 2021, **15**, 16904–16912.

17 Y. Peng, S. Ding, M. Cheng, Q. Hu, J. Yang, F. Wang, M. Xue, Z. Liu, Z. Lin, M. Avdeev, Y. Hou, W. Yang, Y. Zheng and J. Yang, *Adv. Mater.*, 2020, **32**, 2001200.

18 S. Calder, A. V. Haglund, Y. Liu, D. M. Pajerowski, H. B. Cao, T. J. Williams, V. O. Garlea and D. Mandrus, *Phys. Rev. B*, 2020, **102**, 024408.

19 J. Lee, T. Y. Ko, J. H. Kim, H. Bark, B. Kang, S.-G. Jung, T. Park, Z. Lee, S. Ryu and C. Lee, *ACS Nano*, 2017, **11**, 10935–10944.

20 H. L. Zhuang and J. Zhou, *Phys. Rev. B*, 2016, **94**, 195307.

21 A. Louisy, G. Ouvrard, D. M. Schleich and R. Brec, *Solid State Commun.*, 1978, **28**, 61–66.

12472 | *J. Mater. Chem. C*, 2024, **12**, 12468–12473

This journal is © The Royal Society of Chemistry 2024

22 P. Gu, Q. Tan, Y. Wan, Z. Li, Y. Peng, J. Lai, J. Ma, X. Yao, S. Yang, K. Yuan, D. Sun, B. Peng, J. Zhang and Y. Ye, *ACS Nano*, 2020, **14**, 1003–1010.

23 M. Riesner, R. Fainblat, A. K. Budniak, Y. Amouyal, E. Lifshitz and G. Bacher, *J. Chem. Phys.*, 2022, **156**, 054707.

24 S. Kim, S. Yoon, H. Ahn, G. Jin, H. Kim, M.-H. Jo, C. Lee, J. Kim and S. Ryu, *ACS Nano*, 2022, **16**, 16385–16393.

25 S. Kim, J. Lee, C. Lee and S. Ryu, *J. Phys. Chem. C*, 2021, **125**, 2691–2698.

26 S. N. Neal, K. R. O'Neal, A. V. Haglund, D. G. Mandrus, H. A. Bechtel, G. L. Carr, K. Haule, D. Vanderbilt, H.-S. Kim and J. L. Musfeldt, *2D Mater.*, 2021, **8**, 035020.

27 S. Qi, D. Chen, K. Chen, J. Liu, G. Chen, B. Luo, H. Cui, L. Jia, J. Li, M. Huang, Y. Song, S. Han, L. Tong, P. Yu, Y. Liu, H. Wu, S. Wu, J. Xiao, R. Shindou, X. C. Xie and J.-H. Chen, *Nat. Commun.*, 2023, **14**, 2526.

28 R. Diehl and C. D. Carpentier, *Acta Crystallogr., Sect. B: Struct. Crystallogr. Cryst. Chem.*, 1977, **33**, 1399–1404.

29 R. Loudon, *Adv. Phys.*, 1964, **13**, 423–482.

30 J. Kim, J.-U. Lee, J. Lee, H. J. Park, Z. Lee, C. Lee and H. Cheong, *Nanoscale*, 2015, **7**, 18708–18715.

31 M. Kim, S. Han, J. H. Kim, J.-U. Lee, Z. Lee and H. Cheong, *2D Mater.*, 2016, **3**, 034004.

32 Y. Choi, K. Kim, S. Y. Lim, J. Kim, J. M. Park, J. H. Kim, Z. Lee and H. Cheong, *Nanoscale Horiz.*, 2020, **5**, 308–315.

33 S. Kim, J. Lee, G. Jin, M.-H. Jo, C. Lee and S. Ryu, *Nano Lett.*, 2019, **19**, 4043–4051.

This journal is © The Royal Society of Chemistry 2024

J. Mater. Chem. C, 2024, **12**, 12468–12473 | **12473**